

# HA/TCP Compounding of a Porous CaP Biomaterial Improves Bone Formation and Scaffold Degradation—A Long-Term Histological Study

Christian Schopper,<sup>1</sup> Farzad Ziya-Ghazvini,<sup>1</sup> Walter Goriwoda,<sup>1</sup> Doris Moser,<sup>1</sup> Felix Wanschitz,<sup>1</sup> Else Spassova,<sup>2</sup> Georgios Lagogiannis,<sup>1</sup> Alexandra Auterith,<sup>3</sup> Rolf Ewers<sup>1,2</sup>

<sup>1</sup> Department of Cranio-Maxillofacial and Oral Surgery, Medical University of Vienna, Vienna, Austria

<sup>2</sup> Institute of Cranio Maxillo Facial and Oral Rehabilitation Ges.m.b.H., Centre of Tele-Communication and Navigationsurgery, Vienna, Austria

<sup>3</sup> Department of Medical Statistics, Medical University of Vienna, Vienna, Austria

Received 5 July 2004; revised 1 September 2004; accepted 7 September 2004

Published online 23 May 2005 in Wiley InterScience (www.interscience.wiley.com). DOI: 10.1002/jbm.b.30199

**Abstract:** In the present study, two biphasic calcium phosphate biomaterials (BCP) with HA/TCP ratios of 50/50 and 30/70 were obtained from a pure HA biomaterial. The biomaterials which showed the same three-dimensional geometry were implanted into corticocancellous costal defects of sheep. In the specimens of all three biomaterials, abundant bone formation, mineral dissolution from the biomaterial scaffolds, and active cellular resorption of the scaffolds was present after 6 and 12 months. Backscattered electron microscopy showed bone invasion into the pores of the scaffolds and micromechanical interlocking at the bone/biomaterial interface without intervening soft tissue. The pattern of bone formation and scaffold resorption was different for cortical and cancellous bone. No time-based effect, however, was observed. Overall, the BCP biomaterials had formed significantly more bone than the HA biomaterial. Also, scaffold resorption, which was followed by a replacement with newly formed bone, was significantly higher in the BCP biomaterials. Although no significant differences were observed between both BCP biomaterials, the present study had confirmed the assumption that HA/TCP compounding was suitable to improve bone formation and scaffold resorption in the investigated biomaterials and at the same time maintain the osteoconductive properties of the scaffolds. © 2005 Wiley Periodicals, Inc. *J Biomed Mater Res Part B: Appl Biomater* 74B: 458–467, 2005

**Keywords:** bioresorbable; calcium phosphate(s); degradation; histology; bone remodeling

## INTRODUCTION

Calcium phosphate (CaP) biomaterials are widely used as substitutes for autogenous bone grafts when bone reconstruction is considered.<sup>1–3</sup> CaPs such as hydroxyapatite [HA;  $\text{Ca}_{10}(\text{PO}_4)_6(\text{OH})_2$ ] and tricalcium phosphate [TCP;  $\text{Ca}_3(\text{PO}_4)_2$ ] are remarkably biocompatible, provoke little if any inflammatory response, and generally are accepted to be bioactive and osteoconductive when implanted into bone defects.<sup>4–7</sup> The osteoconductive biomaterial serves as a scaffold for new bone formation and increases the ingrowth of osteoprogenitor cells, capillaries, and perivascular tissue from the recipient bed.<sup>8</sup> As a result to biomaterial implantation, newly formed bone ideally is apposed by a direct chemical bonding to the implant surface without intervening soft tis-

sue.<sup>9–11</sup> The extent of new bone formation is influenced by numerous factors such as size, shape, porosity, chemistry, and surface microtexture of the biomaterial.<sup>12</sup>

However, bone reconstruction with nonresorbable material may be potentially associated with long-term tissue reactions and interference with mechanical stress and strain in load-bearing areas.<sup>13–16</sup> Biomaterials should ideally participate in the continuous process of bone remodeling, and the implanted biomaterial should be gradually replaced at a rate comparable to that of ingrowth of newly formed bone.<sup>17</sup>

Different bone formation rates are commonly known between HA and TCP.<sup>18</sup> TCP has been shown to biodegrade more readily than HA, but in an unpredictable way, so that scaffolding for growing bone may be lost too early.<sup>19–22</sup> Biphasic calcium phosphate (BCP) biomaterials consisting of HA and TCP were therefore developed to achieve a better performance in living tissues than pure HA and TCP alone.<sup>23–29</sup>

The suitability of a granular fluorohydroxyapatite biomaterial ( $[\text{Ca}_5(\text{PO}_4)_3\text{OH}_x\text{F}_{1-x}]$ , FHA; FRIOS®Algiore®) to

Correspondence to: C. Schopper (e-mail: christian.schopper@meduniwien.ac.at)

form new bone has been previously shown.<sup>30–32</sup> Biodegradation of the FHA scaffolds was evident but at a slow rate. It was the intent of the present study to obtain a pure HA scaffold and two BCP scaffolds with different ratios of HA/TCP (30/70 and 50/50) with the same three-dimensional geometry as the FHA biomaterial to try to control bone formation and biodegradation of the scaffolds and at the same time maintain their osteoconductive properties. It was assumed that the BCP biomaterials would provide higher bone formation rates while being more readily degraded during bone remodeling than the HA biomaterial that served as control. To prove the accuracy of this assumption, a corticocancellous costal sheep model was used for the implantation of the biomaterials that were retrieved after observation periods of 6 and 12 months, and were evaluated by light microscopy, histomorphometry, and backscattered electron microscopy (BSE).

## MATERIALS AND METHODS

### Biomaterial Preparation

The HA and BCP biomaterials that were investigated in the present study were based on granular calcite scaffolds derived from red algae *corallina officinalis*. For the production of the HA and BCP scaffolds investigated in this study, a standardized process of hydrothermal synthesis had been developed and previously described, which preserves the three-dimensional geometry of the particles of the native algae.<sup>33</sup> To produce the biomaterials intended for the implantation, the natural algal material was subjected to thermal pyrolysis and granulates with particle sizes of 0.5–1 mm were obtained. Temperature was increased from room temperature at a rate of about 25°C/h until a temperature of 700°C was reached and maintained for about 30 h. Thereafter, pyrolyzed algal calcite [Ca<sub>5</sub>CO<sub>3</sub>] scaffolds were subjected to hydrothermal synthesis.

For the transformation of calcite into HA, a stainless steel autoclave lined with thermoplastic polytetrafluoroethylene was used. The calcite scaffolds were suspended in an aqueous solution of ammonium phosphate, and ammonium was added until the pH was set at 9.0. Hydrothermal treatment was carried out over a period of 20 h at a temperature of 300°C and a pressure of 35 atm. After completion of hydrothermal synthesis, the aqueous phase was discarded and the final product was washed and then leached with hot distilled water several times for 1 h each leaching process. Then, the HA scaffolds were dried at 180°C.

For the transformation of calcite into BCP, calcite scaffolds were suspended in an aqueous solution of ammonium phosphate. To suppress the formation of apatite and thus regulate the ratio of HA/TCP, the solution was slightly acidified to a pH of 5.0–6.0. Hydrothermal treatment was then carried out over a period of 20 h at a temperature of 300°C and a pressure of 35 atm, until BCP scaffolds with two defined HA/TCP ratios (30/70 and 50/50) were obtained.

After the leaching process, the BCP scaffolds were dried at 180°C.

### Biomaterial Examination

Samples from all three types of biomaterials were checked for qualitative and quantitative phase composition by X-ray powder diffraction (XRD). From each type of biomaterial, 0.5 g was ground into a fine powder in an agate mortar and loaded into a rotatable specimen holder (sample diameter 16 mm, depth 2 mm). Measurements were taken on a Philips X'Pert PW3050/60 q/q goniometer under the following measurement conditions: CuK $\alpha$  radiation ( $\lambda_1 = 1.54060 \text{ \AA}$ ,  $\lambda_2 = 1.54439 \text{ \AA}$ ), goniometer radius 200 mm, divergence slit  $^{\circ}$ , receiving slit 0.1 mm, secondary bent graphite (002) monochromator, continuous q/2q scans ranging from 5 to 70 $^{\circ}$ , step width 0.02 $^{\circ}$ , 2.0-s measuring time per step. For special Rietveld refinements, the following measurement conditions were preferred:  $2\theta = 5\text{--}140^{\circ}$ , with a measuring time of 5 s step $^{-1}$  and a specimen rotated with four rotations s $^{-1}$ . Determination of the maxima of the measured diffraction profiles and phase identification were performed with routines of the Philips X'Pert data Collector 1.3f software using the Powder Diffraction File (ICDD, International Centre for Diffraction Data, Newtown Square, PA/USA). XRDs of the various samples are shown in Figure 1(a–c).

Also, the three-dimensional geometry of the various types of biomaterial scaffolds was assessed by scanning electron microscopy [JSM 6310, JEOL Ltd., Tokyo, Japan; Figure 2(a–d)]. Biomaterials intended for implantation were filled in batches of 2 mL in glass containers and  $\gamma$ -sterilized. All biomaterials were produced and provided by the Institute of Cranio Maxillo Facial and Oral Rehabilitation, Vienna, Austria.

### Implantation Studies

Six skeletally mature female mountain sheep (age 2–4 years, mean body weight 58.5 kg) were used for the implantation of the biomaterials. Housing and feeding of the animals was performed according to the NIH guidelines for the care and use of laboratory animals. The study protocol was approved by the local Animal Welfare Committee.

For all procedures, the animals were premedicated with ketamine hydrochloride. General anesthesia of the animals was then induced with thiopental and, after endotracheal intubation, maintained with halothane. Supplementary analgesia was obtained by local administration of 2% xylocaine containing epinephrine (1:50,000).

The right hemithorax of each animal was shaved, cleaned with ethanol-iodine, and draped for sterile surgical procedure. After transcutaneous incision and reflection of the periosteum, two ribs were exposed. Six corticocancellous defects (5  $\times$  5 mm) each rib were prepared using a water-cooled dental handpiece and a trephine drill. The biomaterials were mixed separately with 2 mL autogenous venous blood until clotting occurred and thereafter carefully inserted into the created defects, so that four samples of each biomaterial type were placed in each animal. Subsequently, skin and periosteum

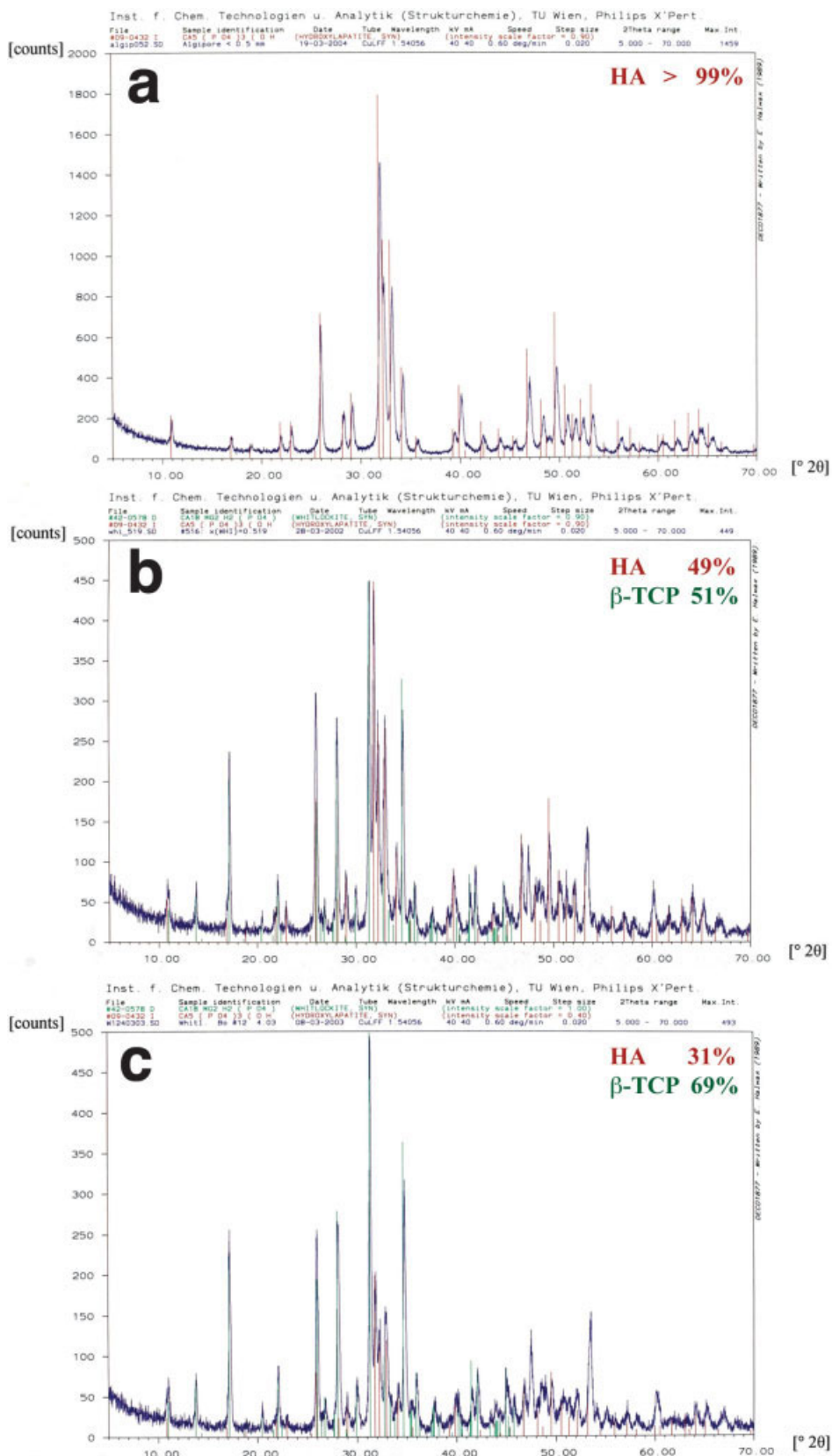


**Figure 1.** Physicochemical characterization of samples from HA (a), 50/50 BCP (b), and 30/70 BCP scaffolds (c). Red patterns denote hydroxyapatite, green patterns denote tricalcium phosphate. XRD imaging, reference phases taken from the Power Diffraction File (ICDD, Newton Square, PA).

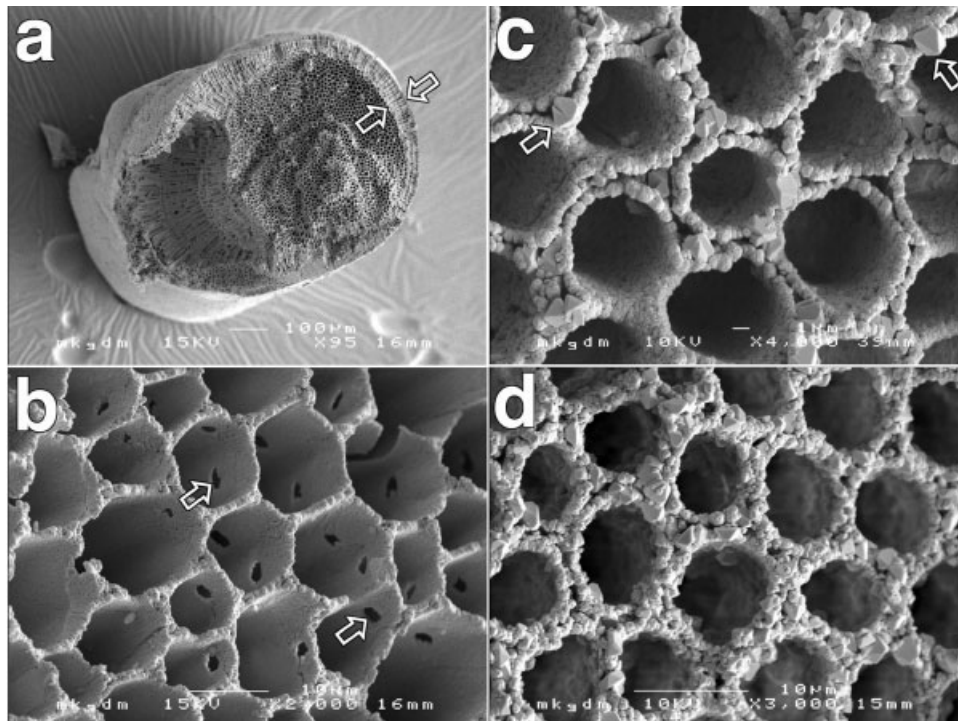


**Figure 2.** (a–d) SEM imaging of the various types of biomaterials. Three-dimensional visualization of a fractured HA-biomaterial (a) particle shows the arrangement of the pores (mean diameter  $10\ \mu\text{m}$ ). Central pores are longitudinally arranged, periodically septated (mean interval  $30\ \mu\text{m}$ ) and interconnectively microperforated (mean diameter of perforations  $1\ \mu\text{m}$ ). Particles are enveloped by a thin but compact cortex (arrows) of orthoradially arranged pores. HA scaffolds (b) are formed by spherical HA crystals; pores are limited by fragile walls with prominent interconnecting microperforations (arrows). 50/50 BCP scaffolds (c) are formed by equal fractions of polyedric TCP (arrows) and spherical HA crystals; walls are thicker and microperforations are less prominent than in HA scaffolds. 30/70 BCP scaffolds (d) are mainly formed by polyedric TCP crystals; the three-dimensional geometry resembles that of 50/50 BCP scaffolds. (a) Bar =  $100\ \mu\text{m}$ ; (b, d) bar =  $10\ \mu\text{m}$ ; (c) bar =  $1\ \mu\text{m}$ .

were repositioned and closed in layers with interrupted resorbable sutures. Animals received standard antibiotic treatment (penicilline, streptomycine) during the first 5 post-operative days; food and water were provided *ad libitum*.

Oxytetracycline ( $25\ \text{mg/kg}$ ; Terramycin®; Pfizer, Vienna, Austria), xylenol-orange-tetrasodium-salt ( $90\ \text{mg/kg}$ ; Merck, Darmstadt, Germany), and 2,7-bis(bis(carboxymethyle)-aminomethyle)-fluoresceine ( $20\ \text{mg/kg}$ ; Calcein®; Merck, Darmstadt, Germany) were administered for fluorochrome bone labeling at biomaterial placement, at 3 months following implantation, and 7 days prior to animal sacrifice, respectively.

Three animals each were sacrificed 6 and 12 months following implantation by infusion of potassium chloride until isoelectric ECG was registered, and the ribs containing the implants were retrieved.

### Sample Preparation

The retrieved ribs were prepared for nondecalcified histology utilizing a modification of the Donath technique.<sup>34</sup> After cleaning from soft tissue and prefixation with 4.5% neutral-buffered formaline for 3 days, the ribs were separated to obtain single segments containing the implanted biomaterial within one surgical defect. These samples were placed in

Schaffer solution (80% ethanol/37% formaline; ratio 2:1) for another 7 days, dehydrated in a graded series of ethanol, and defatted in 100% acetone/100% ethanol (ratio 1:1). The acetone was removed with 100% ethanol, the samples were then placed in 100% methylmethacrylate monomer for 5 days, and thereafter transferred to polymethylmethacrylate and stored at room temperature for 7–15 days. After the resin had cured, two longitudinal sections of each surgical defect containing the implanted biomaterial were obtained with a diamant-coated band saw. Slices were semiautomatically ground down to a thickness of  $50\ \mu\text{m}$  for fluorescence microscopic examination. Finally, slices were further ground down to a thickness of  $5\text{--}10\ \mu\text{m}$  and stained with 1% thionine for light microscopic evaluation. Several specimens of each biomaterial type were also evaluated by BSE microscopy (JSM 6310, JEOL Ltd., Tokyo, Japan).

### Histological Examination

The specimens were examined morphologically with a transmission light microscope (Eclipse 800, Nikon Corp., Tokyo, Japan) and documented microphotographically. For the morphometrical measurements, a digital camera (Sony 950 Power HAD, Sony Corp., Tokyo, Japan) was connected to the microscope, and digitized pictures were measured with an

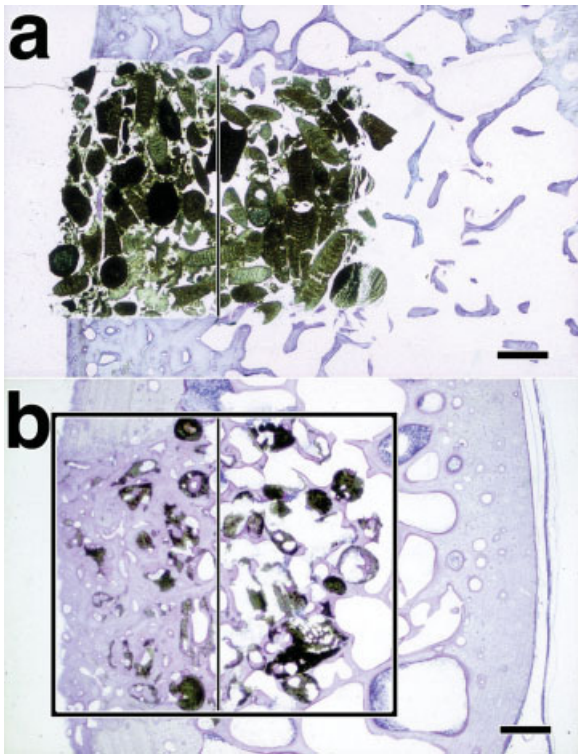


**Figure 3.** (a) Histology of a cadaveric specimen showing configuration and location of a  $5 \times 5$  mm corticocancellous surgical defect containing the biomaterial particles. Particle density resembles that of the postinsertion situs. Vertical line denotes the approximate border between cortical and cancellous bone. Undecalcified specimen, thionine staining. Bar = 1 mm. (b) Histology of a 50/50 BCP specimen 12 months after implantation. A measurement frame as used for morphometrical quantification of bone and biomaterial values from the total surgical defect is shown. Morphometric measurements were also obtained for cortical and cancellous bone compartments alone. Vertical line denotes the approximate border between cortical and cancellous regenerated bone. Newly formed bone shows the same corticocancellous pattern as native bone. Remnants of biomaterial particles are visible in both compartments; biomaterial resorption and replacement was more intense in cortical than in cancellous bone compartments. Undecalcified specimen, thionine staining. Bar = 1 mm.

image analyzing software (Lucia 32G/4.10, Laboratory Imaging Ltd., Prague, Czech Republic) at a magnification of  $4\times$  by a blinded operator. Two longitudinal sections of each surgical defect containing the implanted biomaterial were

measured. The area values for bone and biomaterial were obtained from the total surgical defect [total bone (toBo), total biomaterial (toBm)]. Also, separate measurements were taken for cortical bone compartments [cortical bone (coBo), cortical biomaterial (coBm)] and cancellous bone compartments [cancellous bone (caBo), cancellous biomaterial (caBm)] of the surgical defects. Therefore, the approximate location of the original borderline between cortical and cancellous compartments of the ribs was defined as shown in Figure 3(a, b). Neither automatic nor manual quantification provided a practicable solution for tracing bone portions within intact pores of the particles. These amounts were therefore included into biomaterial area. All area values obtained for statistical analysis comprised the arithmetic mean of its two longitudinal-sectional values.

### Statistical Analysis

For statistical analysis, the arithmetic mean of two longitudinal-sectional values of each surgical defect was used. Several analyses were performed separately for bone and biomaterial. To investigate the differences between bone and biomaterial values obtained from cortical and cancellous bone compartments (coBo, coBm, caBo, and caBm, respectively) for each type of biomaterial, mixed model analysis was performed with the fixed factors *healing time*, *type of biomaterial*, and *bone compartment*. The interactions *healing time*  $\times$  *type of biomaterial*, *type of biomaterial*  $\times$  *bone compartment*, and *healing time*  $\times$  *type of biomaterial*  $\times$  *bone compartment* were analyzed. The random factor *sheep* was included in the model to account for multiple measurements in one sheep. Least-square means were calculated for each *type of biomaterial*, and pairwise comparisons were then performed using a Bonferroni adjustment for the *p*-values.

For the calculation of the bone and biomaterial values obtained from the total surgical defect (toBo and toBm), a similar model as described above was fitted, excluding the fixed factor *bone compartment* and its interactions. *p*-Values  $< 0.05$  were considered to indicate statistical significance. All values are reported as means  $\pm$  standard errors.

## RESULTS

### Histological Results

Histology showed that all bioceramics were correctly implanted. No inflammatory round cell infiltrates due to the

**Figure 5.** (a, b) Comparison of different patterns of biomaterial replacement. Histology showing a cortical and cancellous compartment of a surgical defect in a 50/50 BCP specimen 12 months after implantation. Original outlines of two biomaterial particles are outlined by white lines. In cortical compartments (a), circular scaffold defects are present produced by osteonal bone remodeling; defects show a complete repair by secondarily formed osteons. In cancellous compartments (b), the repair of scaffold portions due to lamellar bone remodeling is incomplete; trabecular remnants of scaffolds are interlocked by newly formed bone trabeculae in a cancellous pattern. Undecalcified specimens, thionine staining. (a, b) Bar =  $100 \mu\text{m}$ . (c, d) Comparison of histological (c) and BSE (d) investigation in a 30/70 BCP specimen 12 months after implantation. Large portions of the biomaterial scaffold have been removed and replaced by secondarily formed osteons during osteonal bone remodeling. BSE imaging shows a micromechanical interlocking at the bone/biomaterial interface and bone ingrowth into the pores; newly formed bone is fully mineralized. Undecalcified specimens, thionine staining in (c). (c, d) Bar =  $100 \mu\text{m}$ .

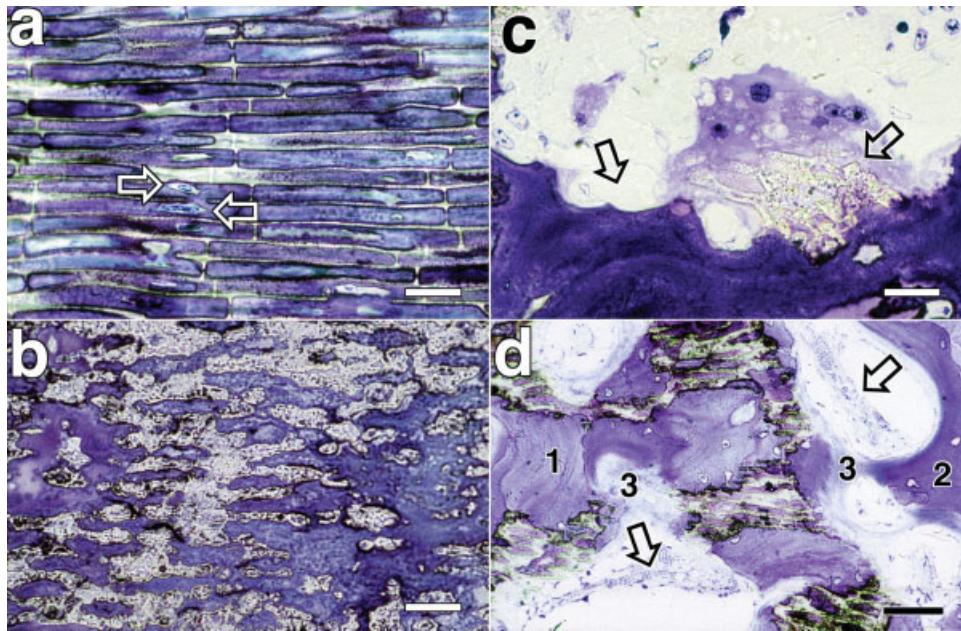


**Figure 4.** (a, b) Comparison of biomaterial degradation in the absence of osteoclastic activity. High power view showing a HA specimen (a) and a 30/70 BCP specimen (b) 6 months after implantation. Intraporous bone is present in both types of biomaterials [note viable osteocytes (arrows) in (a)]. Although the three-dimensional geometry has been retained almost completely in the HA scaffold, biomaterial degradation due to mineral dissolution from the scaffolds is much more pronounced in the 30/70 BCP specimen. Undecalcified specimens, thionine staining. (a, b) Bar = 20  $\mu\text{m}$ . (c) Histology showing active biomaterial resorption in a 30/70 BCP specimen by a multinucleated giant cell during osteoclastic bone remodeling 6 months after implantation. Arrows denote resorption lacunae (left) and incorporated remnants of a particle scaffold (right). Undecalcified specimen, thionine staining. Bar = 20  $\mu\text{m}$ . (d) Histology showing resorbed portions of a 50/50 BCP biomaterial due to osteoclastic bone remodeling 6 months after implantation. Older lamellar bone (1) is present along with woven bone (2). Note that deposition of newly formed unmineralized bone (3) and formation of vasculature (arrows) are closely linked. Undecalcified specimen, thionine staining. Bar = 50  $\mu\text{m}$ .

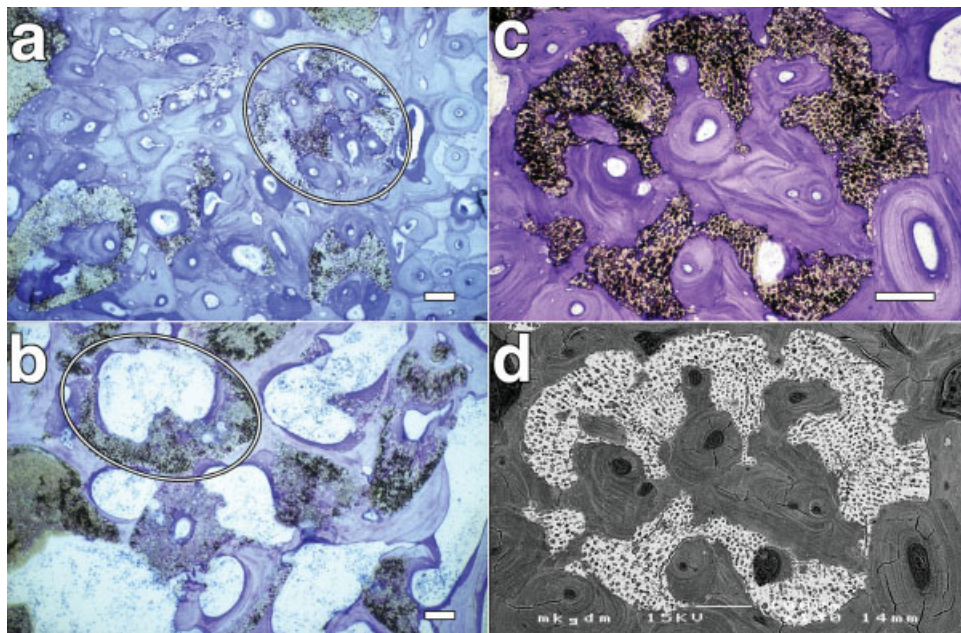


**Figure 5.**

implantation of the biomaterials were observed. The surgical defects included the outer cortical bone of the ribs and cancellous bone [Figure 3(a)]. All defects containing the implanted biomaterials had been repaired by bone promotion from dissected surrounding bone; the biomaterial particles had served as osteoconductive scaffolds [Figure 3(b)]. Bone formed within the surgical defects did not differ in quality between the various types of biomaterials; however, staining was more intense than in surrounding older bone after thionine staining.

At sites of active bone formation, seams of osteoblasts and unmineralized matrix containing collagen fibrils were seen. Incipient mineralization was indicated by calcification fronts. Bone formation was closely linked to angiogenesis [Figure 4(d)].

Bone response to biomaterial implantation was different for cortical and cancellous compartments of the surgical defects. In cortical bone, biomaterial scaffolds were embedded in mature and compact bone that showed an osteonal structure. No intervening soft tissue was present at the bone/biomaterial interface. Bone surrounding the particles showed the presence of Haversian osteonal remodeling after both fluorescence and light microscopy. In cancellous bone, scaffolds were crosslinked by a framework of newly formed bone trabeculae that showed lamellar reinforcement after both light and fluorescence microscopy. Bone had only been incompletely apposed to the scaffolds here; soft tissue and multinucleated giant cells were present where no bone was apposed to the biomaterials. Fibrovascular soft tissue had formed in the marrow cavity, and vasculature was seen near the surfaces of newly formed bone trabeculae.

Histology and BSE imaging showed micromechanical interlocking at the bone/biomaterial interface and bone growth into the pores of the particles in all types of biomaterials. Bone invasion was more intense when particles had been fractured during biomaterial implantation; many particle scaffolds had been completely obstructed by newly formed bone. Moderate vascular ingrowth into the particles was also seen.

Active resorption of particle scaffolds by multinucleated giant cells that functionally resembled osteoclasts was coupled with remodeling of newly formed bone [Figure 4(c)]. Scaffold resorption was evident in all types of biomaterials but was more pronounced in the BCP scaffolds. Resorbed portions had been largely replaced by newly formed bone that had caused a moderate increase in bone mass from 6 to 12 months. The pattern of biomaterial resorption, however, was different for cortical and cancellous compartments of the surgical defects. In cortical bone, defined circular areas of the scaffolds and intraporous bone had been removed by cutting cones from surrounding bone remodeling [Figure 5(a)]. Most of the cortical scaffold defects had been repaired by bone deposited from following closing cones [Figure 5(c, d)]. Osteonal remodeling respected no boundaries, and defects were located in central as well as in peripheral portions of the scaffolds. In cancellous bone, scaffolds and intraporous bone had been resorbed by multinucleated giant cells located in resorption lacunae of bone apposed to the biomaterials. Cancellous bone remodeling respected lamellary boundaries, and

defects were mostly located in the periphery of the scaffolds. Repair by new bone deposition was incomplete in most of the cancellous scaffold defects; biomaterial particles were modeled into trabecular remnants that were integrated into the cancellous structure of the bone/biomaterial mixture by crosslinking bone trabeculae [Figure 5(b)]. In both compartments, remodeling activity and biomaterial replacement had increased from 6 to 12 months. Remodeling activity and biomaterial replacement were more pronounced in the BCP than in the HA scaffolds. Between the 30/70 and 50/50 BCP scaffolds, however, no differences were obvious.

Histology and BSE imaging also showed ultrastructural changes of the biomaterial scaffolds in the absence of osteoclastic activity. Mineral dissolution from the walls of the scaffolds was seen whether the pores of the scaffolds had been obstructed by invading bone or not. Dissolution, however, was more intense when multinucleated giant cells were adherent to the scaffolds. In the BCP scaffolds, mineral dissolution and fragmentation of the scaffolds were more pronounced than in the HA scaffolds [Figure 4(a,b)].

Histomorphometrical results are given in Figure 6.

### Statistical Results

For each type of biomaterial, a significant difference was observed between bone values obtained from cortical and cancellous compartments of the surgical defects (coBo and caBo;  $p < 0.01$ ). Also, a significant difference was present between cortical and cancellous compartments in the various types of biomaterials ( $p < 0.01$ ); the pattern of differences between the biomaterials, however, was similar for cortical and cancellous bone values. In HA biomaterials, significantly lower bone values were present than in 50/50 BCP ( $p < 0.01$ ) and 30/70 BCP biomaterials ( $p < 0.01$ ). 50/50 BCP biomaterials, however, did not differ significantly from 30/70 BCP biomaterials ( $p = 0.93$ ). There was no indication for a difference between the values measured 6 and 12 months following implantation for the various types of biomaterials ( $p = 0.93$ ).

Pearson correlation procedure showed that values for bone and biomaterial were highly negatively correlated ( $-0.93$  at cortical bone compartments and  $-0.59$  at cancellous compartments). Therefore, calculation of the biomaterial values (coBm and caBm) showed similar results to those for bone values.

For bone values obtained from the total surgical defects (toBo), no time-based effect was observed either. Again, significant differences were found between the various types of biomaterials. HA biomaterials showed significantly lower bone values than 50/50 BCP ( $p < 0.01$ ) and 30/70 BCP biomaterials ( $p < 0.01$ ). 50/50 BCP biomaterials, however, did not differ significantly from 30/70 BCP biomaterials ( $p = 0.93$ ). Due to the highly negative correlation between bone and biomaterial values, statistical calculation of the biomaterial values obtained from the total surgical defects (toBm) showed similar results to those for total bone values.

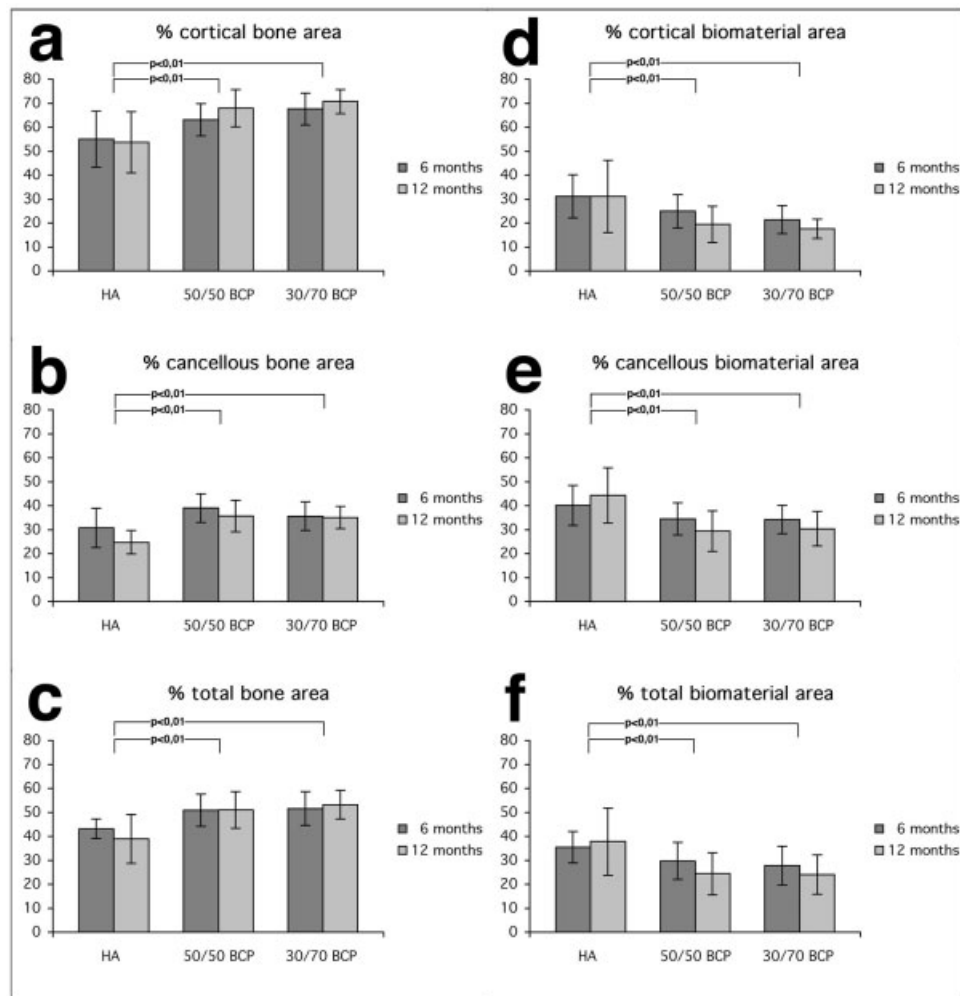


**Figure 6.** Statistical results for cortical, cancellous and total bone area (a–c), and for cortical, cancellous, and total biomaterial area (d–e). Significant differences were present as shown. Cortical and cancellous values for both bone and biomaterial differed significantly in all types of biomaterials after both healing times (not shown). Data were obtained from a total number of 144 specimens (24 each type of biomaterial and healing time). Level of significance was set at  $p < 0.05$ . Values are reported as means  $\pm$  standard errors.

## DISCUSSION

In the present study, bone formation and biomaterial degradation rates of three different granular biomaterials with the same three-dimensional geometry but varying HA/TCP ratios (HA, 50/50 BCP, and 30/70 BCP) were investigated histologically 6 and 12 months following implantation.

CaP biomaterials allow for attachment, proliferation, migration, and phenotypic expression of bone cells leading to bone apposition in direct contact to the biomaterial.<sup>35–37</sup> Noncritical size defects were used in this study to ensure fast and reliable bone healing and to achieve biomaterial replacement at an advanced stage within the observation periods. In defect sizes as employed, healing would have occurred even without biomaterial implantation. Because histological interests were only focused on differences between the various biomaterials, negative controls were not included in this study.

The surgical defects containing the implanted biomaterials had been repaired by appositional bone growth to the particles that served as an osseoconductive scaffold. Bone formation was closely linked to angiogenesis. Pericytes and vascular endothelial cells from ingrowing capillaries<sup>38–40</sup> may have contributed osseoprogenitor cells. New bone had also formed inside the pores in all types of biomaterials. The size range, extent, and interconnectivity of the pores of biomaterials are critical factors affecting diffusion of nutrients, cell attachment, migration, and expression, and tissue ingrowth necessary for bone formation.<sup>41</sup> Although pore sizes of at least 50  $\mu\text{m}$  have been recommended for bone invasion,<sup>42</sup> the suitability of biomaterials with interconnected pore sizes of about 10  $\mu\text{m}$  to allow for the ingrowth of bone *in vivo* has been recently demonstrated.<sup>30</sup> In this study, bone invasion was more pronounced when particles had been fractured during implantation. Bone ingrowth may have been rendered more difficult by a dense cortical layer in intact particles.

Osteoconductivity has been closely related with the chemical composition of biomaterials.<sup>37</sup> For TCP, a trabecular pattern of bone apposition to the particles has been found at cancellous implantation sites, while HA produced a more disseminated pattern.<sup>43</sup> The histological results of this study, however, showed no morphological differences of bone formation between the various types of biomaterials.

Bone formation did not significantly increase from 6 to 12 months; healing times longer than 6 months may not provide a beneficial clinical effect on bone regeneration. Analysis of the data obtained from the total surgical defects showed that the BCP biomaterials had produced significantly more bone than the HA biomaterial. Because biomaterials showed the same three-dimensional geometry, the difference in the bone formation rates must be attributed to the presence of TCP in both BCP biomaterials. Biomaterial dissolution in the body fluids at the implant site may have occurred. For HA, lower solubility and higher stability are known when compared with TCP.<sup>45</sup> In a previous study, we have found mineral dissolution from the walls of the pores in a FHA biomaterial.<sup>30</sup> In this study, mineral dissolution and fragmentation of the scaffold walls in the absence of osteoclastic activity was more pronounced in the BCP than in the HA scaffolds. Enhanced dissolution and accumulation of calcium ions from the walls of the BCP scaffolds at the defect site may have stimulated bone formation.<sup>46</sup> Reprecipitation of apatite has been suggested to be causal for a chemical binding of bone to a biomaterial.<sup>46,47</sup> Whether the intimate bonding of bone to the biomaterials as it was observed in this study comprized micromechanical interlocking, chemical bonding, or a combination of both remains unclear.

TCP has been shown to bioresorb more readily than HA.<sup>19,48–50</sup> We have previously shown active cellular resorption in the scaffolds of a FHA biomaterial.<sup>30</sup> In this study, the BCP biomaterials showed significantly higher scaffold degradation rates than the HA biomaterial. Active resorption of scaffolds during bone remodeling that was followed by a replacement with newly formed bone was observed for all three types of biomaterials. Because of the different patterns of bone formation, bone remodeling, and biomaterial resorption in cortical and cancellous compartments, a corticocancellous structure of the bone/biomaterial mixture had been partly regenerated at the surgical defects; it has been suggested that cortical and cancellous compartments may be considered as two separate functional entities of bone.<sup>44</sup> The higher metabolic activity and bone turnover of cancellous bone, when compared to cortical bone,<sup>51</sup> may also be a reasonable explanation for a reduction of trabecular bone mass from 6 to 12 months, which was present in all types of biomaterials. Cancellous bone healing may have been completed at an early stage after implantation, and newly formed cancellous bone was then reduced by bone remodeling because of the unloaded character of the animal model. Cortical bone mass, in contrast, had moderately increased from 6 to 12 months in the BCP biomaterials but failed to increase in the HA biomaterial. Because bone and biomaterial were strongly negatively correlated ( $r = -0.93$ ) in cortical compartments, a further increase in cortical bone mass was depending on

biomaterial resorption, which was more pronounced in the BCP than in HA scaffolds.

In the present study we have shown that HA/TCP compounding was suitable to improve bone formation and scaffold degradation while the osteoconductive properties of the investigated biomaterials were maintained. Although the differences between HA/TCP ratios of 50/50 and 30/70 failed to reach statistical significance, 30/70 scaffolds were better integrated into physiological bone remodeling. It would be interesting whether a higher percentage of TCP could further increase bone regeneration and biomaterial replacement; currently, HA/TCP ratios of 20/80 and 10/90 are being tested. We will report on the results.

The authors would like to acknowledge the support of the present investigation by the Institute of Cranio Maxillo Facial and Oral Rehabilitation, and wish to thank Dr. Erich Halwax for the X-ray diffraction analyses of all types of biomaterials.

## REFERENCES

1. Hoexter DL. Bone regeneration graft materials. *J Oral Implantol* 2002;28:290–294.
2. Sammarco VJ, Chang L. Modern issues in bone graft substitutes and advances in bone tissue technology. *Foot Ankle Clin* 2002; 7:19–41.
3. Trombelli L, Heitz-Mayfield LJ, Neddleman I, Moles D, Scabbia A. A systematic review of graft materials and biological agents for periodontal intraosseous defects. *J Clin Periodontol* 2002;29:117–135.
4. Jarcho M. Calcium phosphate ceramics as hard tissue prosthetics. *Clin Orthop* 1981;157:259–278.
5. Jarcho M. Biological aspects of calcium phosphates. Properties and applications. *Dent Clin N Am* 1986;30:25–47.
6. de Groot K. Macropore tissue ingrowth: A quantitative and qualitative study on hydroxyapatite ceramics. *Biomaterials* 1986;7:137–143.
7. Muller-Mai CM, Voigt C, Gross U. Incorporation and degradation of hydroxyapatite implants of different surface roughness and surface structure in bone. *Scanning Microsc* 1990;4:613–622.
8. Burchardt, H. The biology of bone graft repair. *Clin Orthop* 1983;174:28–42.
9. Hench LL, Splinter RJ, Allen WC, Greenlee TK. Bonding mechanisms at the interface of ceramic prosthetic materials. *J Biomed Mater Res* 1971;2:117–141.
10. Spector M. Anorganic bovine bone and ceramic analogs of bone mineral as implants to facilitate bone regeneration. *Clin Plast Surg* 1994;21:437–444.
11. Rawlings CE 3rd. Modern bone substitutes with emphasis on calcium phosphate ceramics and osteoinductors. *Neurosurgery* 1993;33:935–938.
12. Monchau F, Lefèvre A, Descamps M, Belquin-Myrdycz A, Laffargue P, Hildebrand HF. In vitro studies of human and rat osteoclast activity on hydroxyapatite,  $\beta$ -tricalcium phosphate, calcium carbonate. *Biomol Eng* 2002;19:143–152.
13. Schliephake H, Lehmann H, Kunz U, Schmelzeisen R. Ultrastructural observations in soft tissues adjacent to titanium plates used in jaw fracture treatment. *Int J Oral Maxillofac Surg* 1993;22:20–25.
14. Rozema FR, de Bruijn WC, Bos RRM, Boering G, Nijenhuis AJ, Pennings AJ. Late tissue response to bone-plates and screws of poly (L-lactide) used for fracture fixation of the zygomatic bone. In: Rozema FR, editor. Resorbable poly (L-lactide) bone plates and screws. PhD Thesis. Germany: University of Groningen, 1991. p 61–79.

15. Assael LA. Discussion: Analysis of reconstruction for anterior mandibular defects using AO plates. *J Oral Maxillofac Surg* 1991;49:1059–1060.
16. Sheen R, MacLeod AM, Mitchell GM, O'Brien BM. Reconstruction of mandibular defects with metallic prostheses and microvascular jejunal autografts. An experimental study. *Br J Plast Surg* 1988;41:138–142.
17. Blokhuis TJ, Wippermann BW, den Boer FC, van Lingen A, Patka P, Bakker FC, Haarman HJTM. Resorbable calcium phosphate particles as a carrier material for bone marrow in an ovine segmental defect. *J Biomed Mater Res* 2000;51:369–375.
18. Fujita R, Yokohama A, Kawasaki T, Kohgo T. Bone augmentation osteogenesis using hydroxyapatite and  $\beta$ -tricalcium phosphate blocks. *J Oral Maxillofac Surg* 2003;61:1045–1053.
19. Egli PS, Miller W, Schenk RK. Porous hydroxyapatite and tricalcium phosphate cylinders with two different pore size ranges implanted in the cancellous bone of rabbits. *Clin Orthop* 1988;232:127–138.
20. Bowers, CM, Vargo JN, Lery B, Emerson JR, Gergquist JJ. Histologic observations following the placement of tricalcium phosphate implants in human infrabony defects. *J Periodontol* 1986;57:286–287.
21. Saffar JF, Colombier ML, Datenville R. Bone formation in tricalcium phosphate filled periodontal infrabony lesions. Histological observations in humans. *J Periodontol* 1990;61:209–216.
22. Schmitz JP, Hollinger JO, Milam SB. Reconstruction of bone using calcium phosphate bone cements: A critical review. *J Oral Maxillofac Surg* 1999;57:1122–1126.
23. Frayssinet P, Troulliet JL, Rouquet N, Azimus E, Autefage A. Osseointegration of macroporous calcium phosphate ceramics having a different chemical composition. *Biomaterials* 1993;14:423–429.
24. Daculsi G, Passutti N, Martin S, Deudon C, LeGeros RZ, Rahe S. Macroporous calcium phosphate ceramic in long bone surgery in human and dogs. Clinical and histological study. *J Biomed Mater Res* 1990;24:391–396.
25. Klein CPAT, de Groot K, Weiqun C, Yubao L, Xingdong Z. Osseous substance formation induced in calcium phosphate ceramics in soft tissues. *Biomaterials* 1994;15:31–34.
26. Nery EB, LeGeros RZ, Lynch KL, Lee K. Tissue response to biphasic calcium phosphate ceramic with different ratios of HA/ $\beta$ -TCP in periodontal osseous defects. *J Periodontol* 1992;68:729–735.
27. Piatelli A, Mangano C, Krajewski A, Ravaglioli A, Martinetti R, Fabri M. Correlation between clinico-histological results and hydroxyapatite phosphate ratio of implanted ceramic granules. In: Anderson OH, Happonan RP, Yli Urpo A, editors. *Bio ceramics*, vol. 7. Butterworth, Heinmann Ltd, Turku, Finland; 1994. p 177–182.
28. Hashimoto-Uoshima M, Ishikawa I, Kinoshita I, Weng HT, Oda S. Clinical and histological observation of replacement of biphasic calcium phosphate by bone tissue in monkeys. *Int J Periodont Restorative Dent* 1995;15:205–213.
29. Piatelli A, Scarano A, Mangano C. Clinical and histologic aspects of biphasic calcium phosphate ceramic (BCP) used in connection with implant placement. *Biomaterials* 1996;17:1767–1770.
30. Schopper C, Moser D, Sabbas A, Lagogiannis G, Spassova E, Koenig F, Donath K, Ewers R. The fluorohydroxyapatite (FHA) FRIOS Algipore is a suitable biomaterial for the reconstruction of severely atrophic human maxillae. *Clin Oral Implants Res* 2003;14:743–749.
31. Ewers R, Goriwoda W, Schopper C, Moser D, Spassova E. Histologic findings at augmented bone areas supplied with two different bone substitute materials combined with sinus floor lifting. Report of one case. *Clin Oral Implants Res* 2004;15:96–100.
32. Watzinger F, Luksch J, Millesi W, Schopper C, Neugebauer J, Moser D, Ewers R. Guided bone regeneration with titanium membranes: A clinical study. *Br J Oral Maxillofac Surg* 2000;38:312–315.
33. Ewers R, Simons B, Kasperk C. Verfahren zur Herstellung eines Hydroxylapatitmaterials. *Int Pat. No. C 01 B 25/32*, 1989.
34. Donath K. Die Trenn-Duennschliff-Technik zur Herstellung histologischer Praeparate von nicht schneidbaren Geweben und Materialien. EXAKT-Kulzer-Druckschrift, Norderstedt; 1988.
35. Boyde A, Corsi A, Quarto R, Cancedda R, Bianco P. Osteoconduction on large macroporous hydroxyapatite ceramic implants: Evidence for a complementary integration and disintegration mechanism. *Bone* 1999;24:579–589.
36. Gatti A, LeGeros RZ, Monari E. Preliminary in vivo evaluation of synthetic CaP materials. In: LeGeros RZ, LeGeros JP, editors. *Bioceramics 11*. Singapore: World Scientific; 1998. p 399–402.
37. Oonishi H, Hench LL, Wilson J, Sugihara F, Tsuji E, Kushitani S, Iwaki H. Comparative bone growth behavior in granules of bioceramic materials of various sizes. *J Biomed Mater Res* 1999;44:31–43.
38. Diaz-Flores L, Gutierrez R, Varela H, Rancel N, Valladares F. Microvascular pericytes: A review of their morphological and functional characteristics. *Histol Histopathol* 1991;6:269–286.
39. Brighton CT, Lorch DG, Kupcha R, Reilly TM, Jones AR, Woodbury RA. The pericyte as a possible osteoblast progenitor cell. *Clin Orthop* 1992;275:287–299.
40. Decker B, Bartel H, Decker S. Relationships between endothelial cells, pericytes, and osteoblasts during bone formation in the sheep femur following implantation of tricalciumphosphate-ceramic. *Anat Rec* 1995;242:310–320.
41. Mankani MH, Kuznetsov SA, Fowler B, Kingman A, Robey PG. In vivo bone formation by human bone marrow stromal cells: Effect of carrier particle size and shape. *Biotechnol Bioeng* 2001;72:96–107.
42. Klawitter JJ. A basic investigation of bone growth in porous materials. Phd Thesis. Clemson, Clemson University; 1979.
43. Gao TJ, Lindholm TS, Kommonen B, Ragni P, Paronzi A, Lindholm TC. Microscopic evaluation of bone-implant contact between hydroxyapatite, bioactive glass and tricalcium phosphate implanted in sheep diaphyseal defects. *Biomaterials* 1995;16:1175–1179.
44. Mundy GR. Bone remodeling and its disorders. Martin Dunitz Ltd., London; 1999.
45. Dorozhkin SV, Epple M. Die biologische und medizinische Bedeutung von Calciumphosphaten. *Angew Chem* 2002;114:3260–3277.
46. Manjubala I, Sivakumar M, Sureshkumar RV, Sastry TP. Bioactivity and osseointegration study of calcium phosphate ceramic of different chemical composition. *J Biomed Mater Res* 2002;63:200–208.
47. Daculsi G. Biphasic calcium phosphate concept applied to artificial bone, implant coating and injectable bone substitute. *Biomaterials* 1998;19:1473–1478.
48. Merry JC, Gibson IR, Best SM, Bonfield W. Synthesis and characterisation of carbonate hydroxyapatite. *J Mater Sci Mater Med* 1998;9:779–784.
49. Yamada S, Heymann D, Bouler JM, Daculsi G. Osteoclastic resorption of calcium phosphate ceramics with different hydroxyapatite/ $\beta$ -tricalcium phosphate ratios. *Biomaterials* 1997;18:1037–1041.
50. Koerten HK, van der Meulen J. Degradation of calcium phosphate ceramics. *J Biomed Mater Res* 1999;44:78–86.
51. Parfitt AM, Mathews CHE, Villanueva AR, Kleerekoper M, Frame B, Rao DS. Relationship between surface, volume, and thickness of iliac trabecular bone in aging and in osteoporosis. *J Clin Invest* 1983;72:1396–1409.